Available online at www.sciencedirect.com
ScienceDirect
Journal of Sound and Vibration 324 (2009) 194–208
JOURNAL OF SOUND AND VIBRATION
www.elsevier.com/locate/jsvi

Free vibration analysis of a circular plate partially in contact with a liquid

Kyeong-Hoon Jeong*, Gyu-Mahn Lee, Tae-Wan Kim

SMART Development Division, Korea Atomic Energy Research Institute, P.O. Box 105, Yuseong, Daejeon 305-600, Republic of Korea

Received 16 May 2008; received in revised form 19 September 2008; accepted 30 January 2009
Handling Editor: L.G. Tham
Available online 17 March 2009

Abstract

This paper provides a theoretical method for a hydroelastic vibration of a clamped circular plate partially in contact with a liquid. It is assumed that the liquid is inviscid and incompressible while the thickness of the plate is small compared to the plate radius, and the gravity effect on the system is neglected. The wet dynamic displacement of the plate is approximated by combining the orthogonal modal functions of a dry circular plate with a clamped boundary condition. The liquid displacement potential satisfying the boundary conditions is derived and the wet dynamic modal functions of the plate are derived by using a compatibility requirement along the contacting surface between the plate and the liquid. The eigenvalue equation for the system is obtained by using the Rayleigh–Ritz method in order to calculate the wet natural frequencies and the mode shapes for the symmetric and the asymmetric modes. The proposed method is verified by observing a good agreement with three-dimensional finite element analysis results. The effects of the liquid thickness and the liquid depth on the natural frequencies are also discussed.

1. Introduction

Free vibration of circular plates in contact with a liquid has been studied recently. Many studies on the subject have been experimentally and theoretically carried out by many researchers such as Kwak [1], Kwak and Kim [2], Chiba [3,4], Amabili and Pasqualini [5], Bauer [6], Amabili and Kwak [7,8], Amabili [9,10], Kwak and Han [11], Cheung and Zhou [12], Jeong [13], Andrianov and Hermans [14], and Jeong and Kim [15]. However all these studies are limited to the case of a fully liquid-contacting circular plate. Circular plates partially in contact with a liquid can be found in various engineering fields such as the compartments of horizontal cylindrical fuel tanks, a circular disk of butterfly valves, and a circular sluice gate, etc. Nevertheless, literature on a partially liquid contacting circular plate cannot be found.

This paper deals with the hydroelastic vibration of a partially liquid-contacting circular plate. Therefore, the purpose of this paper is to develop a theoretical method for the dynamic behavior of a circular plate with a partial wet surface. The circular plate is clamped along the edge of the plate by a rigid cylindrical vessel and

*Corresponding author. Tel.: +82 42 868 8792.
E-mail address: khjeong@kaeri.re.kr (K.-H. Jeong).

0022-460X/$ - see front matter © 2009 Elsevier Ltd. All rights reserved.
doi:10.1016/j.jsv.2009.01.061

one side of the plate is partially in contact with an ideal liquid. It is assumed that the liquid is inviscid and incompressible while the plate thickness is small compared to the plate radius and the gravity effect on the system is neglected. The natural frequencies of the liquid-coupled system are obtained by using the Rayleigh–Ritz method, and they are verified by a three dimensional finite element analysis. The natural frequencies are plotted as a function of the water thickness and as a function of the water level to estimate the relative added mass effect of the liquid.

2. Theoretical background

2.1. Formulation for a circular plate

Fig. 1 represents a circular plate partially in contact with a liquid contained in a rigid cylindrical vessel, where R, h, and d represent the radius, thickness of the circular plate, and the liquid depth, respectively. In the theoretical formulation, the clamped plate with a partial wet surface is considered. The dynamic displacement of the wet plate can be written as a combination of the dry modal functions for the plate and the harmonic time function.

$$w(r,\theta,t)=\sum_{m=0}^{M}\sum_{j=0}^{K}W_{mj}(r,\theta)\exp(\mathrm{i}\omega t)=\sum_{m=0}^{M}\sum_{j=0}^{K}U_{mj}(r)S_{mj}(\theta)\exp(\mathrm{i}\omega t), \tag{1}$$

where the subscript m is the number of nodal diameters of the dry circular plate and the subscript j indicates the number of nodal circles of the plate. The symbol "i" in the equations is used to represent $\sqrt{-1}$ and ω is the natural frequency of the wet circular plate. In order to elucidate the mode shapes and natural frequencies of the plate in contact with the liquid, the Rayleigh–Ritz method is introduced. Therefore, each wet mode shape can be expanded in a series by using a finite number of an admissible functions $U_{mj}(r)$, $S_{mj}(\theta)$ ($m=0,1,2,\ldots,M$; $j=0,1,2,\ldots,K$), and the appropriate unknown coefficients A_{mj}, q_{mj} and p_{mj}.

$$U_{mj}(r)=J_m(\lambda_{mj}r)+A_{mj}I_m(\lambda_{mj}r), \tag{2}$$

$$S_{mj}(\theta)=q_{mj}\cos(m\theta)+p_{mj}\sin(m\theta). \tag{3}$$

In Eq. (2), $J_m(\lambda_{mj}r)$ and $I_m(\lambda_{mj}r)$ are the Bessel function and the modified Bessel function of the first kind, respectively. The admissible function $U_{mj}(r)$ can be assumed as the eigenfunctions of the dry plate which satisfies the boundary condition along its edge. Since the clamped boundary condition of the plate is assumed,

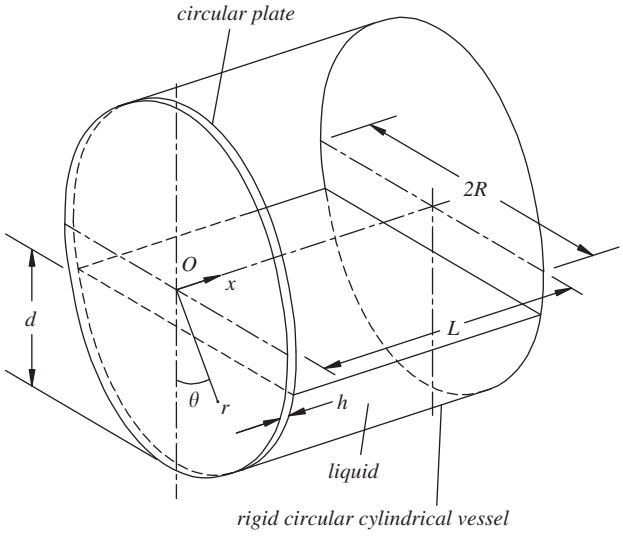

Fig. 1. A circular plate partially in contact with a liquid.

the displacement must be zero along the plate edge, that is, $U_{mj}(r) = 0$ at $r = R$, which yield

$$U_{mj}(r) = J_m(\lambda_{mj}r) - J_m(\lambda_{mj}R)I_m(\lambda_{mj}r)/I_m(\lambda_{mj}R). \tag{4}$$

The frequency parameter for the dry plate, λ_{mj}, can be obtained by using Eq. (4) which satisfies another geometric boundary condition, that is, a zero slope condition along the plate edge, or $\mathrm{d}U_{mj}(r)/\mathrm{d}r = 0$ at $r = R$ as depicted in Ref. [16]:

$$J_m(\lambda_{mj}R)I_{m+1}(\lambda_{mj}R) + J_{m+1}(\lambda_{mj}R)I_m(\lambda_{mj}R) = 0. \tag{5}$$

2.2. Formulation for a liquid motion

The liquid contained in a rigid cylindrical and horizontal vessel is partially filled as shown in Fig. 1. The oscillatory liquid motion in the vessel can be described as the velocity potential satisfying the Laplace equation;

$$\nabla^2\Phi(x, r, \theta, t) = 0. \tag{6}$$

The separation of variables assumes that the velocity potential function $\Phi(x, r, \theta, t)$ can be found as a function of $f(x)$ multiplied by a displacement potential function, $\varphi(r, \theta)$, and a simple harmonic time function, $\exp(\mathrm{i}\omega t)$.

$$\Phi(x, r, \theta, t) = \mathrm{i}\omega\phi(r, \theta, x)\exp(\mathrm{i}\omega t) = \mathrm{i}\omega\varphi(r, \theta)f(x)\exp(\mathrm{i}\omega t). \tag{7}$$

The first derivative of the displacement potential functions, $\phi(r, \theta, x)$ and $\varphi(r, \theta)$, indicates the dynamic displacement of the liquid with respect to the corresponding direction. Eq. (6) can be transformed into two differential equations by Eq. (7).

$$\frac{\varphi(r, \theta)_{,rr} + r^{-1}\varphi(r, \theta)_{,r} + r^{-2}\varphi(r, \theta)_{,\theta\theta}}{\varphi(r, \theta)} = -\frac{f(x)_{,xx}}{f(x)} = -\beta_{ns}^2. \tag{8}$$

When the gravity effect on the liquid motion is neglected, the liquid boundary condition at the free surface can be approximated as the case for a half water level.

$$\varphi(r, \theta)|_{\theta=\pi/2} = \varphi(r, \theta)|_{\theta=-\pi/2} = 0. \tag{9}$$

2.3. Symmetric modes

The liquid motion with respect to $\theta = 0$ can be categorized into two cases, since the liquid-coupled structural system is geometrically symmetric with respect to $\theta = 0$. One is the symmetric modes and the other is the asymmetric ones. The displacement potential function can be separated into the radial function $\zeta(r)$ and the azimuthal function $\psi(\theta)$. The azimuthal displacement potential for the symmetric modes will become

$$\psi(\theta) = \cos[(2n - 1)\theta], \quad n = 1, 2, 3, \ldots, N, \tag{10}$$

in which n is the number of nodal diameters. The displacement potential of the liquid satisfies the approximated liquid boundary condition of Eq. (9). Substituting Eq. (10) into Eq. (8) gives the solutions for the radial and the axial directions.

$$\zeta(r) = B_{ns}J_{2n-1}(\beta_{ns}r) + C_{ns}Y_{2n-1}(\beta_{ns}r), \tag{11}$$

$$f(x) = F_{ns}\sinh(\beta_{ns}x) + G_{ns}\cosh(\beta_{ns}x), \tag{12}$$

where B_{ns}, C_{ns}, F_{ns}, and G_{ns} are the unknown coefficients which can be determined by the boundary conditions and $Y_{2n-1}(\beta_{ns}r)$ is the Bessel function of the second kind. As a rigid wall at $x = L$ is assumed, the displacement of the liquid in the axial direction should vanish at the rigid surface;

$$\left.\frac{\mathrm{d}f(x)}{\mathrm{d}x}\right|_{x=L} = 0. \tag{13}$$

If we now let $r \to 0$, the Bessel function $Y_{2n-1}(\beta_{ns}r)$ tends to be infinite regardless of n. By the way, the displacement potential for the liquid should be finite at $r = 0$ in order to have a physical meaning. Therefore, the unknown coefficient C_{ns} in Eq. (11) must vanish. Finally, the displacement potential satisfying Eq. (13) is reduced to

$$\phi(r,\theta,x) = \sum_{n=1}^{N}\sum_{s=1}^{\infty} F_{ns}\cos[(2n-1)\theta]J_{2n-1}(\beta_{ns}r)\left[\sinh(\beta_{ns}x) - \frac{\cosh(\beta_{ns}x)}{\tanh(\beta_{ns}L)}\right]. \tag{14}$$

Another liquid boundary condition along the radial surface of the rigid cylindrical vessel assures a zero liquid displacement in the radial direction.

$$\left.\frac{\partial\varphi(r,\theta)}{\partial r}\right|_{r=R} = 0. \tag{15}$$

Applying the boundary condition of Eq. (15) to Eq. (14) gives

$$J'_{2n-1}(\beta_{ns}R) = 0. \tag{16}$$

The apostrophe ($'$) of Eq. (16) indicates the derivative with respect to r. The positive coefficient, β_{ns} can be determined by Eq. (16) for every s and n.

The dynamic displacement of the liquid normal to the structure must coincide with that of the structure to satisfy the continuity requirement, so the compatibility condition between the plate and the liquid becomes

$$W_{mj}(r,\theta) = \left.\frac{\partial\phi(r,\theta,x)}{\partial x}\right|_{x=0}. \tag{17}$$

For the symmetric modes, substituting Eqs. (1)–(4) and (14) into Eq. (17) gives

$$\sum_{n=1}^{N}\sum_{s=1}^{\infty}\beta_{ns}F_{ns}\cos[(2n-1)\theta]J_{2n-1}(\beta_{ns}r) = \sum_{m=0}^{M}\sum_{j=0}^{K} q_{mj}\cos(m\theta)\left[J_m(\lambda_{mj}r) - J_m(\lambda_{mj}R)\frac{I_m(\lambda_{mj}r)}{I_m(\lambda_{mj}R)}\right]. \tag{18}$$

In a general case, the wet surface on the circular plate appears as a segment as shown in Fig. 2. When $\theta_0 = \pi/2$, as a particular case, the wet surface forms a semi circle, so the theoretical formulation is available without any approximations for the wet surface region. However, it is very touchy to treat the wet surface segment in the cylindrical coordinates. Therefore, some approximations for the wet surface segment area are necessary for a theoretical formulation for more general case. A wet segment area can be approximated as a bundle of annular sectors so that the wet surface area can be dealt with in the polar coordinates as illustrated in Fig. 2. The radial increment Δr can be written as the total number of the annular sectors, B.

$$\Delta r = (R-d)/B. \tag{19}$$

When an edge angle θ_i and a radius, r_i of an arbitrary i-th annular sector, will be given

$$r_i = R - (i-1)\Delta r, \quad i = 1,2,3,\ldots,B, \tag{20}$$

$$\theta_i = \cos^{-1}\{(R-d)/r_i\}. \tag{21}$$

However, when $\theta = \pi/2$, the segmentation process for the integration is not necessary. Multiplying each term of Eq. (18) by $rJ_{2n-1}(\beta_{ns}r)\cos[(2n-1)\theta]$ and integrating it over $[r_1,\ R]$ and $[-\theta_0,\ \theta_0]$

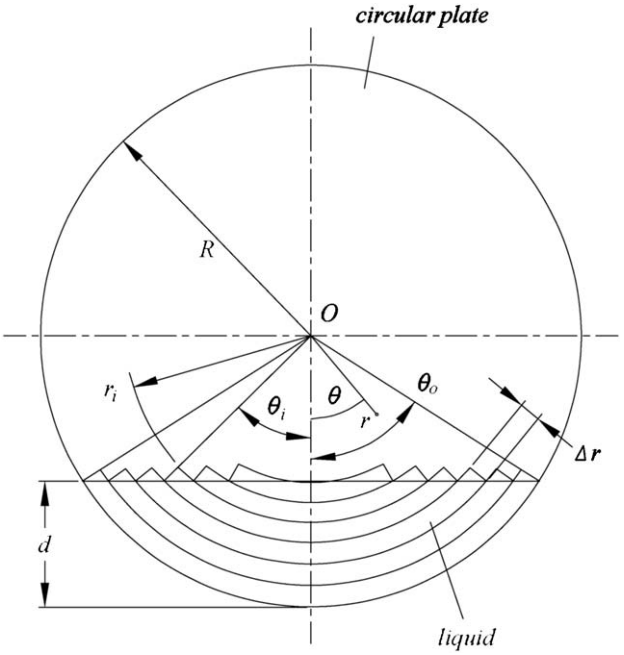

Fig. 2. Wet area segmentation of a circular plate partially in contact with a liquid.

leads to

$$\sum_{i=1}^{B}\int_{r_i}^{r_i+\Delta r}\sum_{s=1}^{\infty}\beta_{ns}F_{ns}r[J_{2n-1}(\beta_{ns}r)]^2\,\mathrm{d}r\int_{-\theta_i}^{\theta_i}\cos^2\{(2n-1)\theta\}\,\mathrm{d}\theta$$
$$=\sum_{i=1}^{B}\int_{r_i}^{r_i+\Delta r}\sum_{m=0}^{M}\sum_{j=1}^{K}\sum_{s=1}^{\infty}q_{mj}r\left[J_m(\lambda_{mj}r)-J_m(\lambda_{mj}R)\frac{I_m(\lambda_{mj}r)}{I_m(\lambda_{mj}R)}\right]J_{2n-1}(\beta_{ns}r)\,\mathrm{d}r$$
$$\times\int_{-\theta_i}^{\theta_i}\cos(m\theta)\cos\{(2n-1)\theta\}\,\mathrm{d}\theta. \tag{22}$$

From the above equation, a relationship between an unknown coefficient for the liquid (F_{ns}) and the unknown coefficient for the plate (q_{mj}) can be obtained.

$$F_{ns}=\sum_{m=0}^{M}\sum_{j=0}^{K}\frac{q_{mj}\Theta_{nmjs}}{\beta_{ns}\Xi_{ns}}, \tag{23}$$

where

$$\Xi_{ns}=\begin{cases}\int_0^R\sum_{s=1}^{\infty}r[J_{2n-1}(\beta_{ns}r)]^2\,\mathrm{d}r\int_{-\pi/2}^{\pi/2}\cos^2\{(2n-1)\theta\}\,\mathrm{d}\theta & \text{for } \theta_0=\frac{\pi}{2}\\ \sum_{i=1}^{B}\int_{r_i}^{r_i+\Delta_r}\sum_{s=1}^{\infty}r[J_{2n-1}(\beta_{ns}r)]^2\,\mathrm{d}r\int_{-\theta_i}^{\theta_i}\cos^2\{(2n-1)\theta\}\,\mathrm{d}\theta & \text{for } \theta_0\neq\frac{\pi}{2},\end{cases} \tag{24}$$

$$\Theta_{nmjs}=\begin{cases}\int_0^R\sum_{s=1}^{\infty}r\left[J_m(\lambda_{mj}r)-J_m(\lambda_{mj}R)\frac{I_m(\lambda_{mj}r)}{I_m(\lambda_{mj}R)}\right]J_{2n-1}(\beta_{ns}r)\,\mathrm{d}r\\ \quad\times\int_{-\pi/2}^{\pi/2}\cos(m\theta)\cos\{(2n-1)\theta\}\,\mathrm{d}\theta \quad \text{for } \theta_0=\pi/2\\ \sum_{i=1}^{B}\int_{r_i}^{r_i+\Delta r}\sum_{s=1}^{\infty}r\left[J_m(\lambda_{mj}r)-J_m(\lambda_{mj}R)\frac{I_m(\lambda_{mj}r)}{I_m(\lambda_{mj}R)}\right]J_{2n-1}(\beta_{ns}r)\,\mathrm{d}r\\ \quad\times\int_{-\theta_i}^{\theta_i}\cos(m\theta)\cos\{(2n-1)\theta\}\,\mathrm{d}\theta \quad \text{for } \theta_o\neq\pi/2.\end{cases} \tag{25}$$

At last, the displacement potential for the symmetric modes will be expressed in terms of q_{mj}.

$$\phi(r,\theta,x)=\sum_{n=1}^{N}\sum_{m=0}^{M}\sum_{j=0}^{K}\sum_{s=1}^{\infty}\frac{q_{mj}\Theta_{nmjs}}{\beta_{ns}\Xi_{ns}}\cos[(2n-1)\theta]J_{2n-1}(\beta_{ns}r)\left[\sinh(\beta_{ns}x)-\frac{\cosh(\beta_{ns}x)}{\tanh(\beta_{ns}L)}\right]. \tag{26}$$

2.4. Asymmetric modes

The displacement potential for the asymmetric modes should also be considered. The azimuthal displacement potential for the asymmetric modes can be written as Eq. (27) to satisfy the approximate liquid boundary condition of Eq. (9).

$$\phi(\theta)=\sin(2n\theta),\quad n=1,2,3,\ldots,N. \tag{27}$$

Similarly, we can obtain the displacement potential for the asymmetric modes.

$$\phi(r,\theta,x)=\sum_{n=1}^{N}\sum_{s=1}^{\infty}F_{ns}\sin(2n\theta)J_{2n}(\beta_{ns}r)\left[\sinh(\beta_{ns}x)-\frac{\cosh(\beta_{ns}x)}{\tanh(\beta_{ns}L)}\right]. \tag{28}$$

As one applies the boundary condition of Eq. (17) to Eq. (28), the transcendental equation for the asymmetric modes can be obtained

$$J'_{2n}(\beta_{ns}R)=0. \tag{29}$$

Therefore, the positive coefficient, β_{ns} for the asymmetric modes will also be determined by Eq. (29). By substituting Eqs. (1)–(4) and (28) into Eq. (17), for the asymmetric modes, the compatibility condition becomes

$$\sum_{n=1}^{N}\sum_{s=1}^{\infty}\beta_{ns}F_{ns}\sin(2n\theta)J_{2n}(\beta_{ns}r)=\sum_{m=1}^{M}\sum_{j=1}^{K}p_{mj}\sin(m\theta)\left[J_m(\lambda_{mj}r)-J_m(\lambda_{mj}R)\frac{I_m(\lambda_{mj}r)}{I_m(\lambda_{mj}R)}\right]. \tag{30}$$

Multiplying each side of Eq. (30) by $rJ_{2n}(\beta_{ns}r)\sin(2n\theta)$ and integrating it over $[R-d,\ R]$ and $[-\theta_0,\ \theta_0]$ gives

$$\begin{aligned}&\sum_{i=1}^{B}\int_{r_i}^{r_i+\Delta r}\sum_{s=1}^{\infty}\beta_{ns}F_{ns}r[J_{2n}(\beta_{ns}r)]^2\,\mathrm{d}r\int_{-\theta_i}^{\theta_i}\sin^2(2n\theta)\,\mathrm{d}\theta\\&=\sum_{i=1}^{B}\int_{r_i}^{r_i+\Delta r}\sum_{m=1}^{M}\sum_{j=1}^{K}\sum_{s=1}^{\infty}p_{mj}r\left[J_m(\lambda_{mj}r)-J_m(\lambda_{mj}R)\frac{I_m(\lambda_{mj}r)}{I_m(\lambda_{mj}R)}\right]J_{2n}(\beta_{ns}r)\,\mathrm{d}r\\&\times\int_{-\theta_i}^{\theta_i}\sin(m\theta)\sin(2n\theta)\,\mathrm{d}\theta.\end{aligned} \tag{31}$$

Hence the unknown coefficient for the liquid motion, F_{ns} can be written in terms of the another unknown coefficient p_{mj} from Eq. (31).

$$F_{ns}=\sum_{m=1}^{M}\sum_{j=1}^{K}\frac{p_{mj}\Omega_{nmjs}}{\beta_{ns}\Lambda_{ns}}, \tag{32}$$

where

$$\Lambda_{ns}=\begin{cases}\int_0^R\sum_{s=1}^{\infty}r[J_{2n}(\beta_{ns}r)]^2\,\mathrm{d}r\int_{-\theta_0}^{\theta_0}\sin^2(2n\theta)\,\mathrm{d}\theta & \text{for } \theta_0=\pi/2\\ \sum_{i=1}^{B}\int_{r_i}^{r_i+\Delta r}\sum_{s=1}^{\infty}r[J_{2n}(\beta_{ns}r)]^2\,\mathrm{d}r\int_{-\theta_i}^{\theta_i}\sin^2(2n\theta)\,\mathrm{d}\theta & \text{for } \theta_0\neq\pi/2,\end{cases} \tag{33}$$

$$\Omega_{nmjs} = \begin{cases} \int_0^R r\left[J_m(\lambda_{mj}r) - J_m(\lambda_{mj}R)\dfrac{I_m(\lambda_{mj}r)}{I_m(\lambda_{mj}R)}\right]J_{2n}(\beta_{ns}r)\,\mathrm{d}r \\ \quad \times \int_{-\theta_0}^{\theta_0} \sin(m\theta)\,\sin(2n\theta)\,\mathrm{d}\theta \quad \text{for } \theta_0 = \pi/2 \\ \sum_{i=1}^{B} \int_{r_i}^{r_i+\Delta r} r\left[J_m(\lambda_{mj}r) - J_m(\lambda_{mj}R)\dfrac{I_m(\lambda_{mj}r)}{I_m(\lambda_{mj}R)}\right]J_{2n}(\beta_{ns}r)\,\mathrm{d}r \\ \quad \times \int_{-\theta_i}^{\theta_i} \sin(m\theta)\sin(2n\theta)\,\mathrm{d}\theta \quad \text{for } \theta_0 \neq \pi/2. \end{cases} \tag{34}$$

Finally, the displacement potential for the asymmetric modes is rewritten in terms of the unknown coefficient of the plate, p_{nj}.

$$\phi(r,\theta,x) = \sum_{n=1}^{N}\sum_{m=1}^{M}\sum_{j=1}^{K}\sum_{s=1}^{\infty} \frac{p_{nj}\Omega_{nmjs}}{\beta_{ns}\Lambda_{ns}} \sin(2n\theta)J_{2n}(\beta_{ns}r)\left[\sinh(\beta_{ns}x) - \frac{\cosh(\beta_{ns}x)}{\tanh(\beta_{ns}L)}\right]. \tag{35}$$

2.5. Rayleigh–Ritz method

The symmetric and the asymmetric vibration modes appear with respect to $\theta = 0$ for the wet condition. A sufficiently large finite number of terms, M and K, must be considered to obtain a converged solution, and a vector $\mathbf{q}$ of the unknown coefficients is introduced in order to perform numerical calculations:

$$\mathbf{q} = \{q_{00}\ q_{01}\ q_{02}\ \cdots\ q_{0K}\ q_{10}\ q_{11}\ q_{12}\cdots\ q_{MK}\}^{\mathrm{T}} \quad \text{for the symmetric modes with respect to } \theta = 0, \tag{36}$$

$$\mathbf{q} = \{p_{11}\ p_{12}\ p_{13}\ \cdots\ p_{1K}\ p_{21}\ p_{22}\ p_{23}\ \cdots\ p_{MK}\}^{\mathrm{T}} \quad \text{for the asymmetric modes with respect to } \theta = 0. \tag{37}$$

The reference kinetic energy of the vibrating plate for the symmetric and the asymmetric vibration modes can be expressed as

$$T_K^* = \frac{\rho h}{2}\int_0^{2\pi}\int_0^R \mathbf{q}^{\mathrm{T}} r W_{mj} W_{pk}\mathbf{q}\,\mathrm{d}r\,\mathrm{d}\theta = \rho h \mathbf{q}^{\mathrm{T}}\mathbf{Z}\mathbf{q}, \tag{38}$$

where

$$Z_{(u,v)} = \begin{cases} \pi R^2\{J_m(\lambda_{mj}R)\}^2\delta_{uv} & \text{for } m = 0 \\ \dfrac{\pi R^2}{2}\{J_m(\lambda_{mj}R)\}^2\delta_{uv} & \text{for } m > 0 \end{cases} \tag{39}$$

and δ_{uv} is the Kroneker delta. The subscripts u and v in Eq. (39) can be defined as Eqs. (40) and (41).

$$u = Mm + j, \quad v = Kp + k. \tag{40,41}$$

The maximum potential energy of the vibrating plate is written approximately as

$$V_K \approx \frac{D(\lambda_{mj})^2(\lambda_{pk})^2}{2}\int_0^{2\pi}\int_0^R r W_{mj} W_{pk}\,\mathrm{d}r\,\mathrm{d}\theta = D\mathbf{q}^{\mathrm{T}}\mathbf{H}\mathbf{q}, \tag{42}$$

where

$$H_{(u,v)} = \begin{cases} \dfrac{\pi}{R^2}(\lambda_{mj}R)^4\{J_m(\lambda_{mj}R)\}^2\delta_{uv} & \text{for } m = 0 \\ \dfrac{\pi}{2R^2}(\lambda_{mj}R)^4\{J_m(\lambda_{mj}R)\}^2\delta_{uv} & \text{for } m > 0. \end{cases} \tag{43}$$

The reference kinetic energy of the contained liquid can be calculated by an integration along the wet surface of the plate.

$$T_F^* = \begin{cases} -\dfrac{\rho_0}{2}\sum_{p=0}^{M}\sum_{k=0}^{K} q_{pk}\int_{-\pi/2}^{\pi/2}\int_0^R r W_{pk}\phi(r,\theta,0)\,\mathrm{d}r\,\mathrm{d}\theta & \text{for } \theta_0 = \pi/2 \\ -\dfrac{\rho_0}{2}\sum_{p=0}^{M}\sum_{k=0}^{K} q_{pk}\sum_{i=1}^{B}\int_{-\theta_i}^{\theta_i}\int_{r_i}^{r_i+\Delta r} r W_{pk}\phi(r,\theta,0)\,\mathrm{d}r\,\mathrm{d}\theta & \text{for } \theta_0 \neq \pi/2. \end{cases} \tag{44}$$

For the symmetric modes, substituting Eqs. (1)–(4), (26) into Eq. (44) gives

$$T_F^* = \begin{cases} \dfrac{\rho_0}{2}\sum_{n=1}^{N}\sum_{p=0}^{M}\sum_{k=0}^{K} q_{pk}\int_{-\pi/2}^{\pi/2}\int_0^R \cos(p\theta) r\left[J_p(\lambda_{pk}r) - J_p(\lambda_{pk}R)\dfrac{I_p(\lambda_{pk}r)}{I_p(\lambda_{pk}R)}\right] \\ \quad \times \sum_{m=0}^{M}\sum_{j=0}^{K}\sum_{s=1}^{\infty}\dfrac{\cos\{(2n-1)\theta\}J_{2n-1}(\beta_{ns}r)}{\beta_{ns}\Xi_{ns}\,\tanh(\beta_{ns}L)} q_{mj}\Theta_{nmjs}\,\mathrm{d}r\,\mathrm{d}\theta & \text{for } \theta_0 = \pi/2 \\ \dfrac{\rho_0}{2}\sum_{n=1}^{N}\sum_{p=0}^{M}\sum_{k=0}^{K} q_{pk}\sum_{i=1}^{B}\int_{-\theta_i}^{\theta_i}\int_{r_i}^{r_i+\Delta r} \cos(p\theta) r\left[J_p(\lambda_{pk}r) - J_p(\lambda_{pk}R)\dfrac{I_p(\lambda_{pk}r)}{I_p(\lambda_{pk}R)}\right] \\ \quad \times \sum_{m=0}^{M}\sum_{j=0}^{K}\sum_{s=1}^{\infty}\dfrac{\cos\{(2n-1)\theta\}J_{2n-1}(\beta_{ns}r)}{\beta_{ns}\Xi_{ns}\,\tanh(\beta_{ns}L)} q_{mj}\Theta_{nmjs}\,\mathrm{d}r\,\mathrm{d}\theta & \text{for } \theta_0 \neq \pi/2. \end{cases} \tag{45}$$

By performing an integration of Eq. (45), we can obtain the reference kinetic energy as a matrix form.

$$T_F^* = \frac{\rho_0}{2}\sum_{n=1}^{N}\sum_{p=0}^{M}\sum_{k=0}^{K} q_{pk}\sum_{m=0}^{M}\sum_{j=0}^{K} q_{mj}\sum_{s=1}^{\infty}\frac{\Theta_{npks}\Theta_{nmjs}}{\beta_{ns}\Xi_{ns}\,\tanh(\beta_{ns}L)} = \rho_0\mathbf{q}^{\mathrm{T}}\mathbf{G}\mathbf{q}, \tag{46}$$

where

$$G_{(u,v)} = \sum_{n=1}^{N}\sum_{s=1}^{\infty}\frac{\Theta_{npks}\Theta_{nmjs}}{2\beta_{ns}\Xi_{ns}\,\tanh(\beta_{ns}L)}. \tag{47}$$

Similarly, the reference kinetic energy of the liquid for the asymmetric vibration modes, will be written as

$$T_F^* = \frac{\rho_o}{2}\sum_{n=1}^{N}\sum_{p=1}^{M}\sum_{k=1}^{K} q_{pk}\sum_{m=1}^{M}\sum_{j=1}^{K} q_{mj}\sum_{s=1}^{\infty}\frac{\Xi_{npks}\Xi_{nmjs}}{\beta_{ns}\Lambda_{ns}\,\tanh(\beta_{ns}L)} = \rho_0\mathbf{q}^{\mathrm{T}}\mathbf{G}\mathbf{q}, \tag{48}$$

where

$$G_{(u,v)} = \sum_{s=1}^{\infty}\sum_{n=1}^{N}\frac{\Xi_{npks}\Xi_{nmjs}}{2\beta_{ns}\Lambda_{ns}\,\tanh(\beta_{ns}L)}. \tag{49}$$

The relationship between the reference total kinetic energy multiplied by its square circular frequency and the maximum potential energy is used in order to calculate the wet natural frequencies. Minimizing the Rayleigh quotient with respect to the unknown parameters $\mathbf{q}$, the eigenvalue equation is obtained.

$$D\mathbf{H}\mathbf{q} - \omega^2\{\rho h\mathbf{Z} + \rho_0\mathbf{G}\}\mathbf{q} = \{0\}. \tag{50}$$

Determinant of the left side in Eq. (50) must be zero to obtain a non-trivial solution, and the natural frequency ω of the wet plate can be calculated.

3. Numerical example and discussion

3.1. Theoretical and finite element model

A numerical example test was solved by using commercial software, Mathcad (release 14). The eigenvalues of Eq. (50) were calculated to demonstrate the accuracy of the Rayleigh–Ritz method for a circular plate

partially in contact with a liquid. The derived frequency equation involves an infinite and finite series of algebraic terms. In the theoretical calculation, the expansion term s was set at 50, the expanding terms M and K for the admissible functions were set at 7, and the expanding term for the liquid motion N was set at 11 to obtain a converged solution. It is obvious that the accuracy of the results depends on the size of the truncated matrices and the number of series expanding terms. The lowest 10 natural frequencies of the half liquid-contacting circular plate were given in Table 1 as a function of the number of considered admissible functions. It was observed that the only seven terms of the admissible functions could give the converged results within the lowest 10 natural frequencies. The number of the annular sectors for the segmentation of the liquid contacting area was $B = 20$ for the 25 percent water level.

In order to check on the validity of the theory, a circular plate partially in contact with water was examined by a finite element analysis using a commercial computer code, ANSYS (release 10.0). Three dimensional finite element models for the 50 and 25 percent water levels were constructed as shown in Fig. 3.

It was assumed that the circular plate was made of aluminum with a radius of 240 mm and a thickness of 3 mm. The inner radius of the cylindrical vessel was identical to that of the plate. The liquid thickness was 80 mm for the 50 percent water level and the liquid thickness was 200 mm for the 25 percent water level. The physical properties of the plate and the liquid used in the theoretical calculation and the finite element analysis

Table 1
Convergence test for natural frequencies of a circular plate with a half wet surface ($L = 80$ mm).

Serial mode	Natural frequency (Hz)				
	$j = m = 3$	$j = m = 4$	$j = m = 5$	$j = m = 6$	$j = m = 7$
1	45.57	45.56	45.55	45.55	45.55
2	118.31	118.26	118.22	118.27	118.24
3	153.51	152.05	152.02	151.98	151.98
4	256.02	229.30	226.48	226.39	226.26
5	284.58	276.57	276.30	276.67	276.37
6	–	281.17	280.78	280.74	280.73
7	414.54	382.79	377.10	377.25	377.13
8	–	–	440.03	421.92	421.08
9	–	445.13	443.71	443.61	443.51
10	–	–	–	498.20	497.58

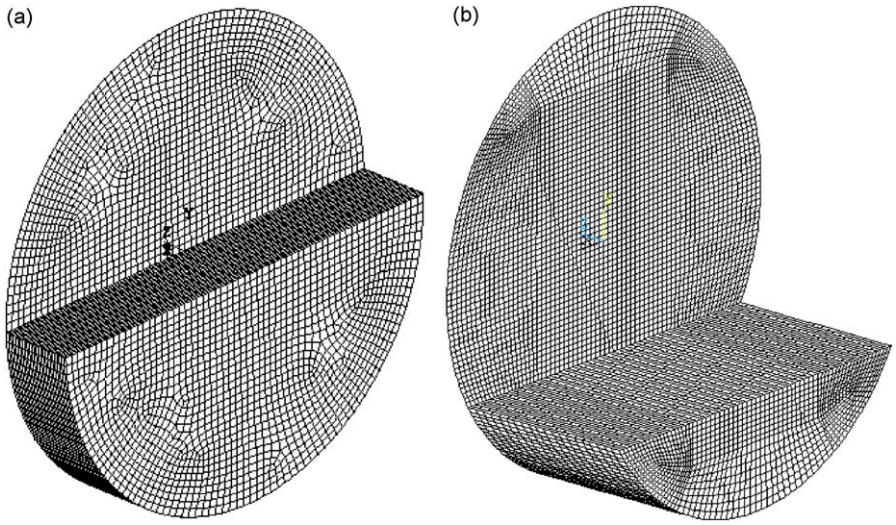

Fig. 3. Three-dimensional finite element models of a liquid-contacting circular plate with a partial wet surface ($R = 240$ mm): (a) 50% water level ($L = 80$mm) and (b) 25% water level ($L = 200$mm).

were as follows: Young's modulus = 69.0 GPa, Poisson's ratio = 0.3, plate mass density = 2700 kg/m^3, and liquid density = 1000 kg/m^3. The viscosity of the liquid was neglected in both the theoretical calculation and the finite element analysis.

Finite element analysis using ANSYS was performed to obtain the natural frequencies of the circular plate partially in contact with water. For the finite element analysis, a three dimensional model was constructed with liquid elements (FLUID80) and elastic shell elements (SHELL63). The liquid region was divided into a number of liquid elements and the plate region was also meshed with shell elements. The liquid movement at $r = R$, namely along the rigid vessel wall, was restricted to the radial direction only, on the other hand, no restrictions were imposed on the other directions. The liquid at the top surface could move freely in any direction. Hence, a sloshing at the top surface of the liquid was allowed. The liquid movement at $x = L$, namely at the rigid side wall, was also restricted to the axial direction. The axial displacement of the liquid nodes adjacent to the surface of the wetted circular plate coincided with those of the plate so that the finite element model could simulate Eq. (17). The clamped circular plate was divided into 2884 quadrilateral elastic shell elements, and the liquid region of the finite element model consisted of 40 376 hexahedral liquid elements, for the 50 percent water level, and the model for the 25 percent water level was composed of 4640 elastic shell elements and 28480 liquid elements as illustrated in Fig. 3. A clamped boundary condition along the plate edge was applied in the finite element model. The natural frequencies of 50 modes were obtained by the Block Lanczos-iteration extraction technique in order to extract the eigenvalues and eigenvectors in the finite element analysis.

Table 2
Natural frequencies of a circular plate with a half wet surface ($L = 80$ mm).

Serial mode	Mode shape category	Natural frequency (Hz)		Discrepancy (%)
		Theory	FEM	
1	Symmetric	45.6	45.5	0.22
2	Asymmetric	118.2	117.9	0.25
3	Symmetric	151.9	151.4	0.33
4	Symmetric	226.3	225.7	0.26
5	Asymmetric	276.1	274.4	0.62
6	Symmetric	280.7	280.6	0.04
7	Asymmetric	376.8	376.0	0.21
8	Symmetric	421.1	418.8	0.55
9	Asymmetric	443.4	443.0	0.09
10	Symmetric	497.6	495.9	0.34

Table 3
Natural frequencies of a circular plate with a liquid depth $d = R/2$ (25% liquid level, $L = 200$ mm).

Serial mode	Mode shape category	Natural frequency (Hz)		Discrepancy (%)
		Theory	FEM	
1	Symmetric	119.1	120.5	−1.16
2	Symmetric	206.4	206.1	0.15
3	Asymmetric	256.2	257.6	0.54
4	Symmetric	372.1	353.1	5.38
5	Asymmetric	357.3	358.1	−0.22
6	Symmetric	446.3	468.6	−4.75
7	Asymmetric	532.4	524.3	1.54
8	Symmetric	523.3	534.6	−2.11
9	Symmetric	629.4	633.6	−0.66

3.2. Theoretical and finite element results

The wet natural frequencies of the plate are listed in Table 1 within the 10th serial mode number. It was found that the theoretical natural frequencies agreed with the finite element results to within a 1 percent discrepancy for the 50 percent water level and within ± 6 percent for the 25 percent water level as listed in Tables 2 and 3, respectively. These results show that the suggested theoretical method was verified for engineering applications. Especially, the theoretical results for the 50 percent water level could accurately predict the finite element analysis results. However, some discrepancies were observed between the theoretical

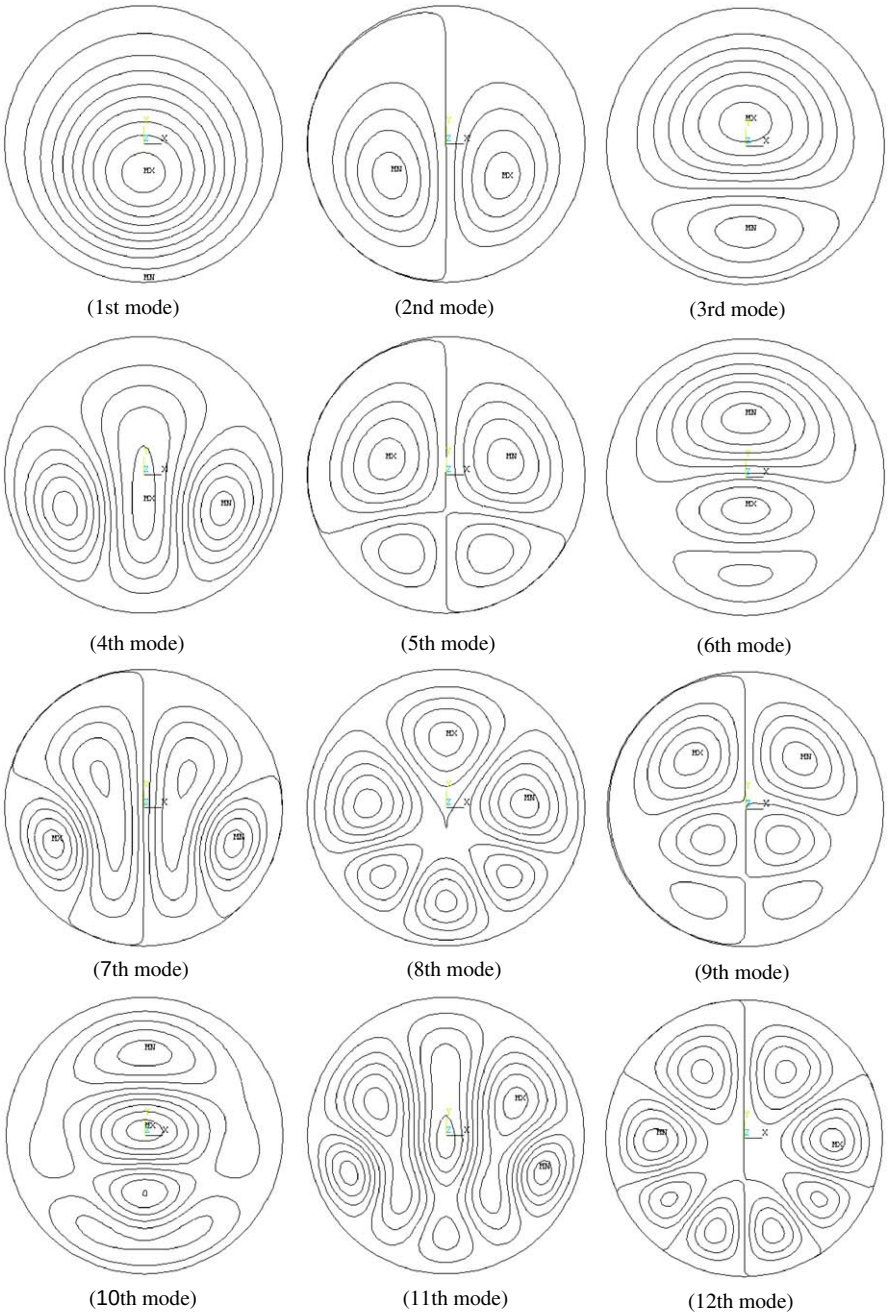

Fig. 4. Typical mode shapes of the circular plate with a half wet surface (finite element analysis result, $L = 80$ mm).

results and the finite element analysis results. These discrepancies seem to be caused by the approximation of the boundary condition at the liquid free surface, a lack of an orthogonality in Eqs. (22) and (31), and the segmentation in the wet area.

The fundamental frequency of the dry plate was 129.6 Hz, but that of the wet plate with an 80 mm water thickness was 45.5 Hz. Therefore, the frequency reduction due to the added mass effect was about 65 percent. This reduction in the frequency depends on the liquid thickness, the liquid depth and the vibration modes. As the wet mode shapes are basically different from the dry ones, that is to say, the wet modes are so complicated that the wet modes cannot be defined with the number of nodal circles and the nodal diameters, it is very difficult for the wet modes to become homologous to the dry modes one by one. So, it seems to be meaningless that the natural frequency of the wet modes is normalized with respect to that of the dry modes, or the non-dimensional added virtual mass increment (NAVMI) factors are introduced in this problem.

3.3. Mode shapes

The mode shapes of the plate in contact with water are illustrated in Fig. 4. All the mode shapes can be categorized as symmetric modes and asymmetric modes with respect to $\theta = 0$. In Fig. 4, the first mode, third mode, fourth mode, sixth mode, … etc. are the symmetric modes. On the contrary, the others such as the second mode, fifth mode, seventh mode, ninth mode, … etc. correspond to the asymmetric modes. All the wet mode shapes are distorted from the original dry mode shapes. For example, the second and third modes originate from the dry mode with one nodal line and a zero nodal circle. These two modes will be identical to the mode with one nodal diameter and a zero nodal circle, if the plate is in the dry condition. However, as the concentrated liquid mass in the lower part of the plate causes a different added mass effect on each mode, it produces two independent modes. Similar phenomenon happens at the fourth and the sixth modes. The fifth mode is equivalent to the dry mode with two nodal diameters and a zero nodal circle, and the eighth mode

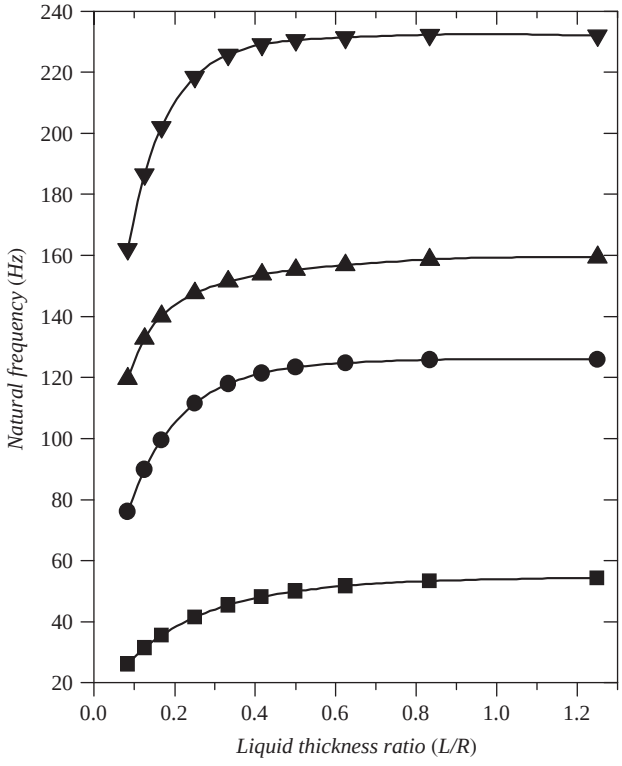

Fig. 5. Effect of water thickness on natural frequencies of the circular plate in contact with water (—■—, first mode; —●—, second mode; —▲—, third mode; —▼—, fourth mode).

stem from the dry mode with three nodal diameters and a zero nodal circle. The fourth and fifth modes in Fig. 4 originate from the dry mode shape with two nodal diameters and a zero nodal circle. The dry mode is bifurcated into two different modes due to the unevenly distributed liquid mass along the plate. Additionally the mode shapes are distorted from the original dry mode which is familiar to us. The ninth mode in Fig. 4 also demonstrates another distorted mode shape which stems from the dry mode shape with one nodal diameter and one nodal circle. It was also observed that the liquid thickness does not significantly affect the mode shapes even though the natural frequencies are increased with the liquid thickness.

3.4. Effects of the liquid thickness and the liquid depth

It is well known that the wet natural frequencies of a structure in contact with water are sensitive to the liquid thickness when the liquid thickness is particularly small. The effect of the liquid thickness between the circular plate and the rigid side wall on the natural frequencies is plotted in Fig. 5 for the half-liquid contacting case. A narrow gap tends to reduce the wet natural frequencies for all the modes. When the liquid thickness ratio (L/R) is greater than approximately 1.0, the natural frequencies are converged to the values of the infinite liquid thickness case as shown in Fig. 5. For the higher modes, it seems that the natural frequencies of the wet plate are converged to the infinite liquid case when the liquid thickness ratio is greater than approximately 0.5.

Figs. 6 and 7 show the effect of the liquid depth, d on the normalized natural frequencies. The wet natural frequencies were normalized with respect to the corresponding dry natural frequencies. The figures show that the natural frequencies decrease with the water level. The natural frequencies of the fundamental, second and third modes drastically decrease along the 20–60 percent liquid level, since the clamped plate dynamic deformation is maximized in the range of the liquid level. The second and third modes are an identical mode in the dry condition and the fully liquid contacting condition (100 percent liquid level) as shown in Fig. 6. However, the symmetric mode with respect to $\theta = 0$ has a transition plateau owing to a stagnation of the hydrodynamic mass increment induced by the coincidence of the nodal line and the water level. Fig. 7

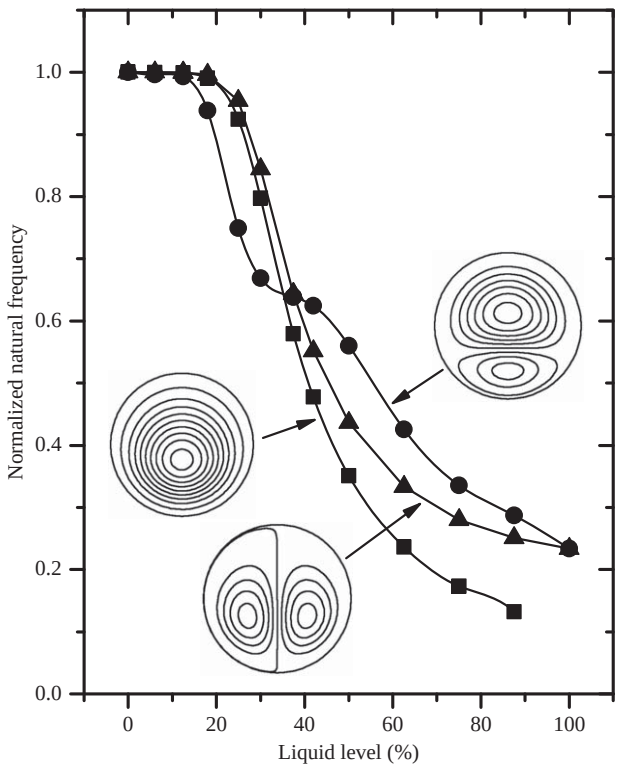

Fig. 6. Effect of water depth on natural frequencies of the circular plate (—■—, first mode; —●—, second mode; —▲—, third mode).

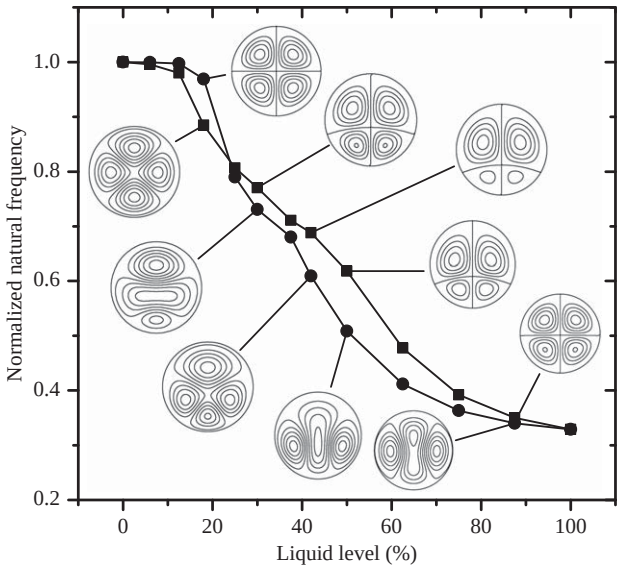

Fig. 7. Effect of the liquid depth on natural frequencies of the circular plate (—■—, fourth mode; —●—, fifth mode).

illustrates a transition of the mode shape with a zero nodal circle and two nodal diameters from a regular dry mode shape to the bifurcated and distorted mode shapes.

4. Conclusions

A theoretical method to estimate the natural frequencies of a circular plate partially in contact with a liquid was developed by the Rayleigh–Ritz method. It was verified that the theoretical approach based on an ideal liquid assumption and a half liquid-contacting clamped plate can predict the coupled natural frequencies well. Two types of vibration modes, namely, the symmetric and the asymmetric modes were observed, which are distorted from the original dry mode shapes. It was evident that the wet vibration mode shapes were not significantly changed regardless of the liquid thickness even though the natural frequencies were increased with the liquid thickness. It was also observed that the wet natural frequencies of the plate increase with the liquid thickness and they decrease with the liquid depth. A dry mode shape is bifurcated into a symmetric shape and an asymmetric shape according to an increase of the water depth, and eventually it returns to its original dry shape for the fully liquid-filled case.

References

[1] M.K. Kwak, Vibration of circular plates in contact with water, *Transaction of the American Society of Mechanical Engineers, Journal of Applied Mechanics* 58 (1991) 480–483.
[2] M.K. Kwak, K.C. Kim, Axisymmetric vibration of circular plates in contact with fluid, *Journal of Sound and Vibration* 146 (1991) 381–389.
[3] M. Chiba, Axisymmetric free hydroelastic vibration of a flexural bottom plate in a cylindrical tank supported on an elastic foundation, *Journal of Sound and Vibration* 169 (1994) 387–394.
[4] M. Chiba, The influence of elastic bottom plate motion on the resonant response of a liquid free surface in a cylindrical container, *Journal of Sound and Vibration* 202 (1997) 417–426.
[5] M. Amabili, A. Pasqualini, Natural frequencies and modes of free-edge circular plates vibrating in vacuum or in contact with liquid, *Journal of Sound and Vibration* 188 (1995) 685–699.
[6] H.F. Bauer, Coupled frequencies of a liquid in a circular cylindrical container with elastic liquid surface cover, *Journal of Sound and Vibration* 180 (1995) 689–704.
[7] M. Amabili, M.K. Kwak, Free vibration of circular plates coupled with liquids: revising the Lamb problem, *Journal of Fluids and Structures* 10 (1996) 743–761.

[8] M. Amabili, M.K. Kwak, Vibration of circular plates on a free fluid surface: effect of surface waves, *Journal of Sound and Vibration* 226 (1999) 407–424.
[9] M. Amabili, Effect of finite fluid depth on the hydroelastic vibrations of circular and annular plates, *Journal of Sound and Vibration* 193 (1996) 909–925.
[10] M. Amabili, Vibrations of circular plates resting on a sloshing liquid: solution of the fully coupled problem, *Journal of Sound and Vibration* 245 (2001) 261–283.
[11] M.K. Kwak, S.B. Han, Effect of fluid depth on the hydroelastic vibration of free-edge circular plate, *Journal of Sound and Vibration* 230 (2000) 171–185.
[12] Y.K. Cheung, D. Zhou, Hydroelastic vibration of a circular container bottom plate using the Galerkin method, *Journal of Fluids and Structures* 16 (2002) 561–580.
[13] K.H. Jeong, Free vibration of two identical circular plates coupled with bounded fluid, *Journal of Sound and Vibration* 260 (2003) 653–670.
[14] A.I. Andrianov, A.J. Hermans, Hydroelasticity of a circular plate on water of finite or infinite depth, *Journal of Fluids and Structures* 20 (2005) 719–733.
[15] K.H. Jeong, K.J. Kim, Hydroelastic vibration of a circular plate submerged in a bounded compressible fluid, *Journal of Sound and Vibration* 283 (2005) 153–172.
[16] R.D. Blevins, *Formulas for Natural Frequency and Mode Shapes*, Van Nostrand Reinhold Company, London, 1979 Table 11-1.